SUPPLEMENTARY INFORMATION **Gassmann et al.**

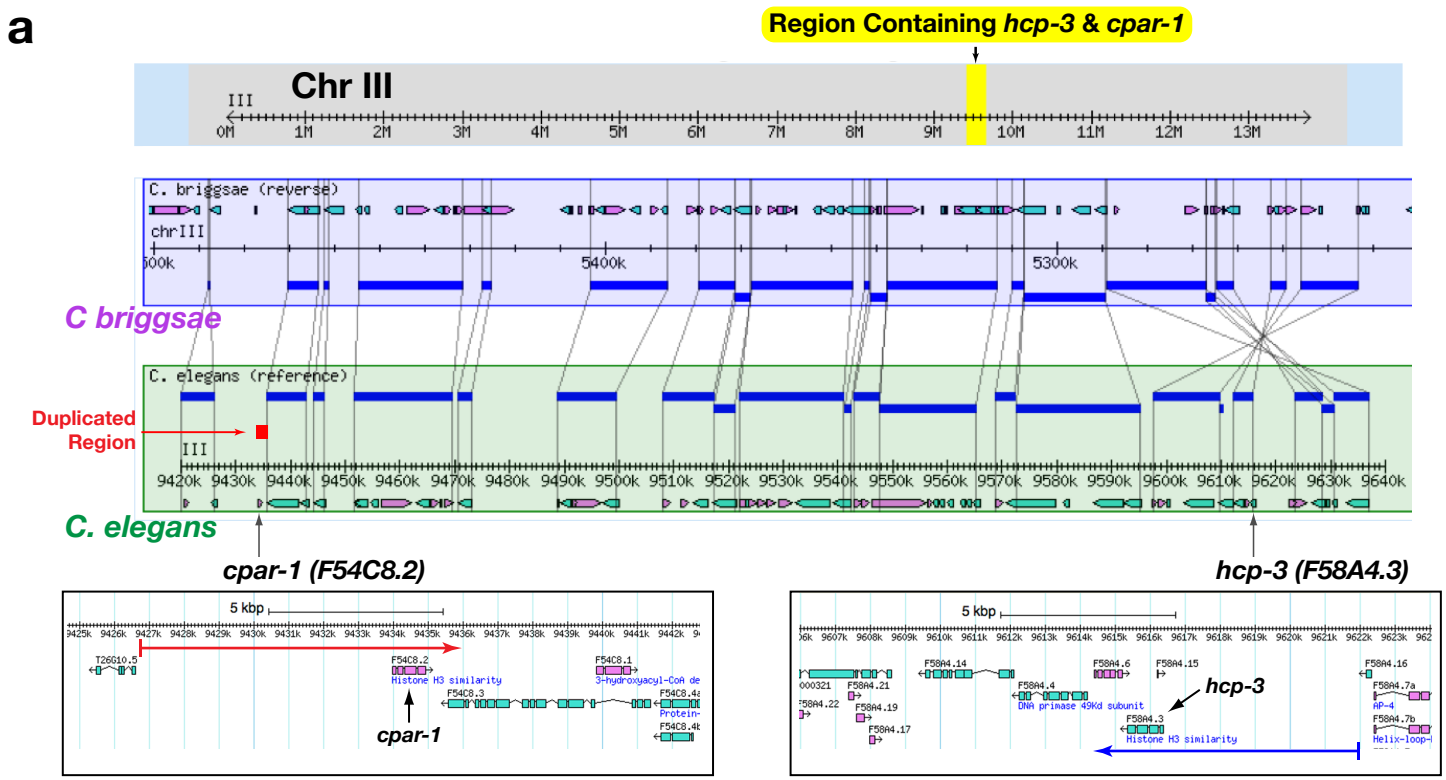

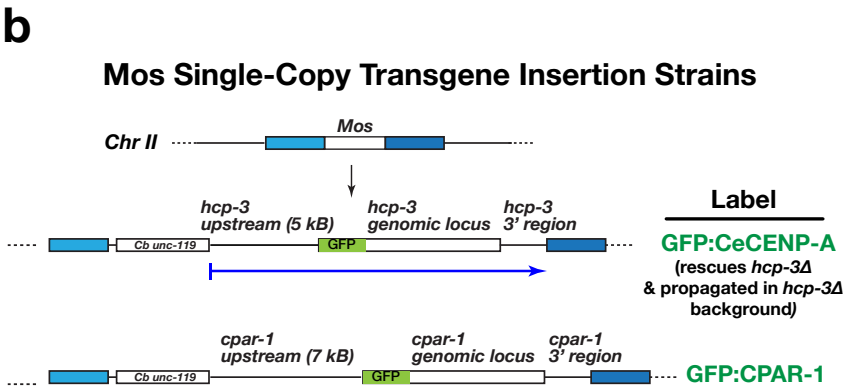

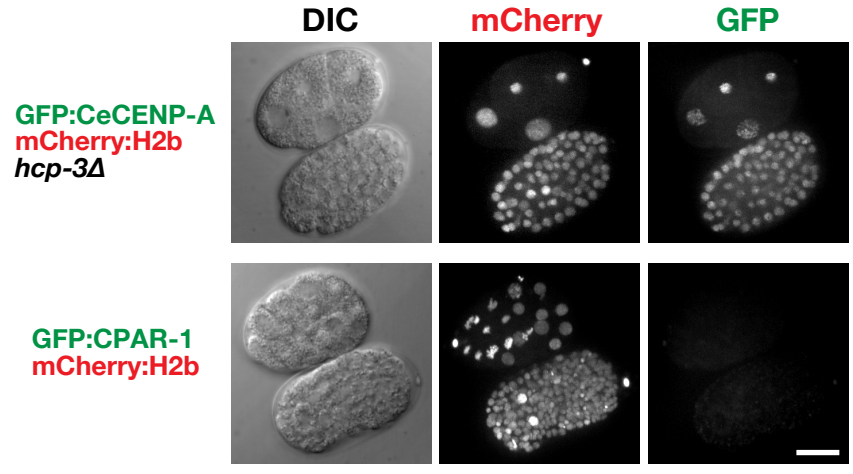

Figure S1: Of the two *C. elegans* CENP-A-like proteins HCP-3 and CPAR-1, only HCP-3 (= CeCENP-A) is present in embryos.

(a) Synteny map of *C. elegans* and *C. briggsae*, the most closely related nematode to *C. elegans* with a fully sequenced genome. *cpar-1* is not present in *C. briggsae*. In conjunction with nucleotide sequence analysis, the synteny map suggests that *cpar-1* is the product of a recent duplication event (the duplicated region is marked in red) in the *C. elegans* lineage. In previous work, we had characterized the specificity of antibodies, protein levels of HCP-3 and CPAR-1, and cross-depletion by dsRNAs[8].

(b) Constructs used for Mos-based stable single-copy integration2 of GFP-tagged transgenes to visualize HCP-3 and CPAR-1 in living embryos and adult worms. Both fusion proteins are expressed under control of their endogenous promoter and 3' regions, which are marked in blue and red, respectively, in *(a)*. The *gfp:hcp-3* transgene fully rescues the *hcp-3* deletion allele *ok1892 (hcp-3 Δ/CeCENP-AΔ)*. All experiments involving the *gfp:hcp-3* strain were performed in the deletion background.

For clarity, and to facilitate communication, we refer to HCP-3 as CeCENP-A throughout the primary manuscript text and figures and in all subsequent supplementary figures.

(c) Embryos dissected from worms expressing GFP:CeCENP-A and GFP:CPAR-1. Chromatin is marked by *pie-1*-driven mCherry:histone H2b. GFP:CeCENP-A is present in the nuclei of all cells but there is no detectable GFP:CPAR-1 signal at any stage of embryogenesis. Images were acquired using identical imaging conditions in living embryos. Scale bar, 10 μm.

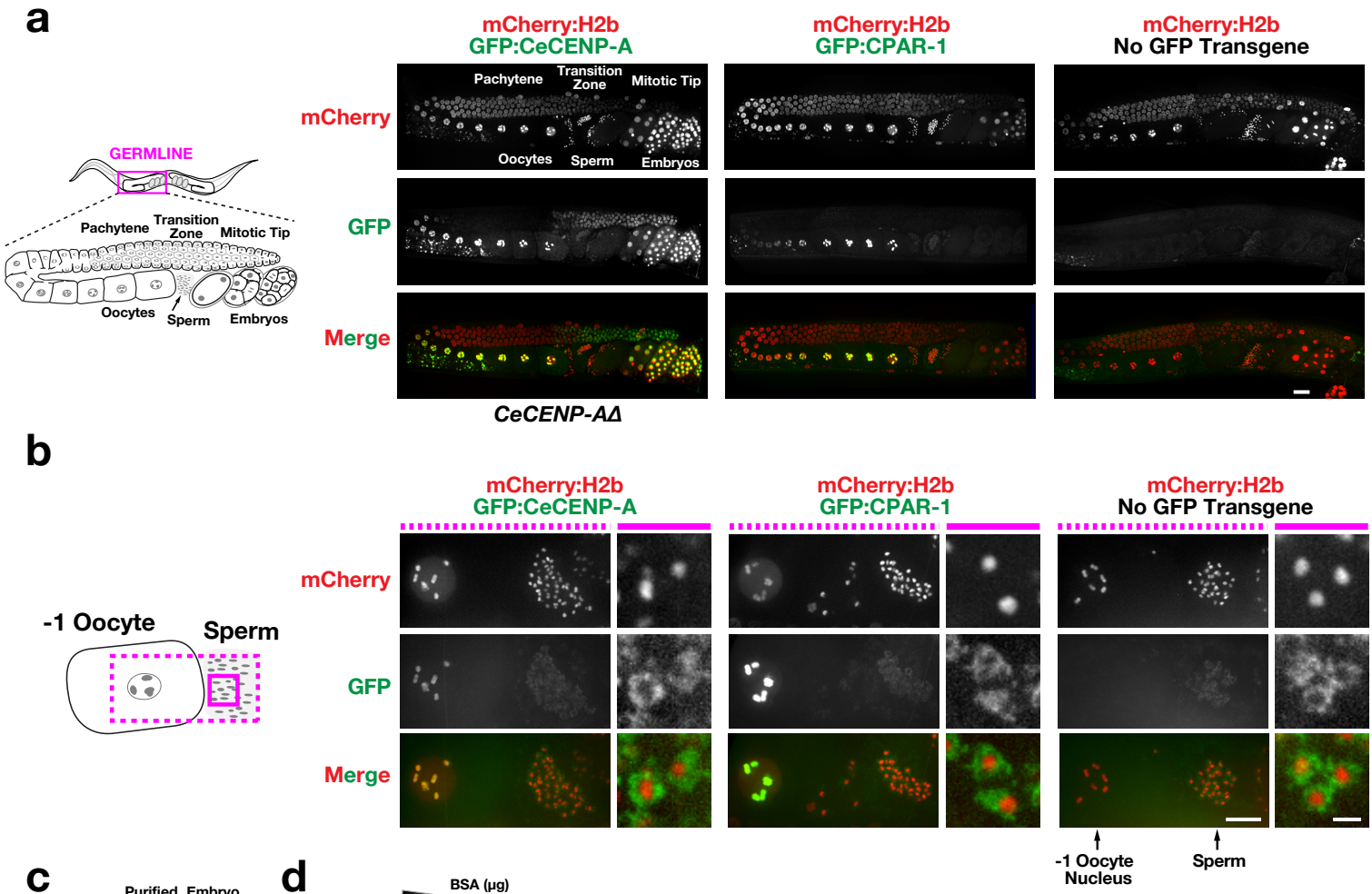

Figure S2: CPAR-1 expression is restricted to the diplotene/diakinesis stages in the maternal germline and neither CPAR-1 nor CeCENP-A is detectable in sperm.
(a) *Schematic*: view of the adult hermaphrodite gonad, where cells divide at the mitotic tip, enter the meiotic program, and progress through meiosis I prophase as they move through the gonad arm towards the spermatheca. After oocytes are fertilized by sperm, two meiotic divisions and the early embryonic divisions take place in utero. Images show the gonad region of adult hermaphrodites expressing GFP:CeCENP-A (in a *CeCENP-AΔ* background) or GFP:CPAR-1 from single-copy integrated transgenes as described in *Fig. S1c*. Chromatin is marked by *pie-1*-driven mCherry:histone H2b. GFP:CeCENP-A is expressed at the mitotic tip and the transition zone, is not detectable in nuclei during the pachytene stage, and re-appears at the turn of the gonad with robust chromosomal localization in oocytes and embryos. In contrast, GFP:CPAR-1 is undetectable until the turn of the gonad (*diplotene*), is highly expressed in maturing oocytes (*diakinesis*), but completely absent from embryos (see also *Fig. S1c*). Neither GFP:CeCENP-A nor GFP:CPAR-1 are detectable in sperm (the diffuse signal is due to non-nuclear autofluorescence as it is also present in a strain lacking any GFP transgene). Scale bar, 20 µm.
(b) Images of the -1 oocyte and the spermatheca in adult hermaphrodites expressing GFP:CeCENP-A or GFP:CPAR-1 together with mCherry:histone H2b. A strain expressing only mCherry:histone H2b was imaged as a control. Both proteins are detected on bivalent chromosomes in the -1 oocyte (the oocyte immediately adjacent to the spermatheca) but no signal above non-nuclear autofluorescence is detected in sperm. Scale bar, 10 µm; higher magnification view, 2 µm.
All images were acquired using identical imaging conditions in living worms without fixation or antibody staining.
(c) The specialized architecture of amoeboid *C. elegans* sperm, which lack actin and tubulin cytoskeletons, precludes the use of a conventional loading control in immunoblots. Shown here instead is a Coomassie-stained protein gel of a purified sperm sample compared with embryo extract. The arrow marks the major sperm proteins. Sperm concentration was measured by microscopy following DAPI staining and 3.3 x the amount of purified sperm in the lane shown here were loaded for the immunoblot in *Fig. 1b*.
(d) 6xHis:CeCENP-A standard used for quantitative immunoblotting (*Fig. 1b; Fig. 2e*). The bacterially expressed fusion protein was purified using nickel affinity under denaturing conditions and electroelution following SDS-PAGE. The concentration of the purified protein was quantified relative to a BSA standard.

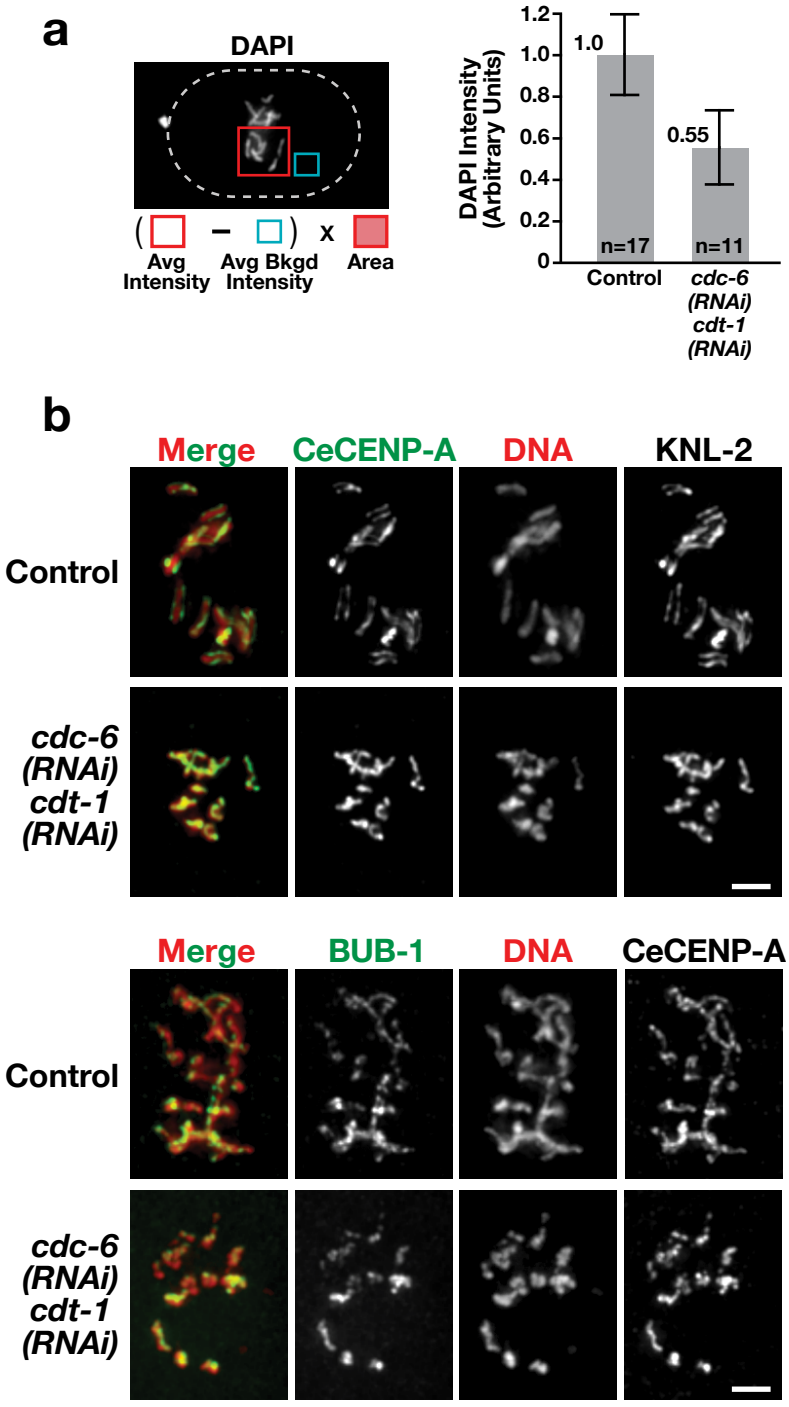

Figure S3: CeCENP-A loading on chromatin in one-cell embryos can occur in the absence of DNA replication.
(a) Quantitation of DNA content in one-cell embryos following RNAi-mediated depletion of the DNA replication factors CDC-6 and CDT-1. The intensity of DAPI-stained chromatin, measured in the first mitotic division as indicated, confirmed successful inhibition of replication.
(b) Immunofluorescence analysis in one-cell embryos following inhibition of DNA replication, showing that CeCENP-A and its loading factor KNL-2 localize normally to mitotic chromosomes and are able to recruit the outer kinetochore component BUB-1. Scale bars, 2 μm.

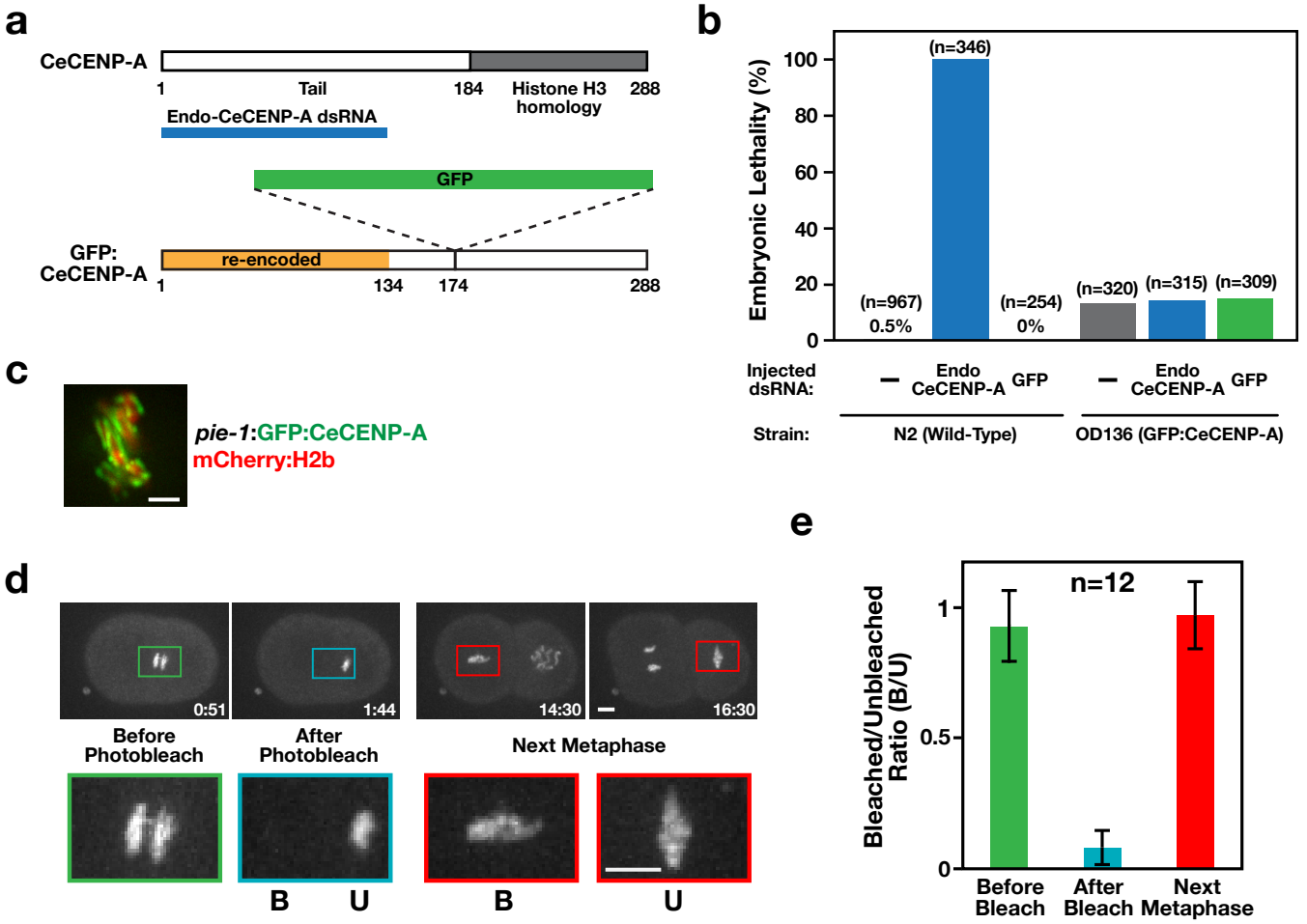

Figure S4: An RNAi-resistant internal GFP fusion of CeCENP-A rescues embryonic lethality caused by a dsRNA targeting both CeCENP-A and CPAR-1 and fully turns over on chromatin between successive early embryonic divisions.

(a) *Schematic*: construct used to generate a GFP:CeCENP-A transgenic strain by ballistic bombardment. The transgene encoding the fusion was constructed in the context of the genomic CeCENP-A locus and expressed under control of the *pie-1* promoter and 3' region. The orange-shaded region was re-encoded to preserve coding information but make the transgene resistant to RNAi. The dsRNA corresponding to this region is referred to as Endo (for endogenous) CeCENP-A dsRNA and depletes endogenous CeCENP-A as well as the fluorescence signal of GFP:CPAR-1 observed in oocytes1 (CPAR-1 cannot be detected by immunoblotting).

(b) Embryonic viability of wild-type N2 worms versus strain OD136, generated by random integration of the construct described in *(a)* using ballistic bombardment, following injection of Endo-CeCENP-A dsRNA or a dsRNA targeting GFP. Strain OD136 exhibits ~13% lethality associated with the transgene insertion site – this conclusion is based on segregation of the lethality with the transgene in multiple outcrosses and no reduction in the lethality following GFP RNAi, despite loss of the GFP signal. The Endo-CeCENP-A dsRNA leads to 100% lethality in N2 worms but no significant increase above the ~13% lethality associated with the insertion site in OD136, indicating that the transgene-encoded fusion rescues the lethality. The RNAi-resistant transgene also rescues the "kinetochore null" phenotype associated with CeCENP-A depletion in the one-cell embryo (not shown). As CPAR-1 is also targeted by the Endo-CeCENP-A dsRNA, these results suggest that CPAR-1 is not required for viability and does not have any discernable function in embryonic chromosome segregation.

(c) Prometaphase image of the GFP:CeCENP-A fusion described in *(a)* together with mCherry:histone H2b. Scale bar, 2 μm.

(d) Representative images from a photobleaching experiment analogous to the one shown in *Fig. 1e*. In these experiments, no *par-6(RNAi)* was performed and hence natural developmental asynchrony causes the metaphase plates in the 2-cell embryo to form ~2 min apart. Higher magnification views highlight bleached *(B)* and unbleached *(U)* chromosome sets. Scale bars, 5 μm.

(e) Quantitation of photobleaching experiments. Error bars are 95% confidence intervals for the means. This result is consistent with the experiment shown in *Fig. 1e* and *1f*.

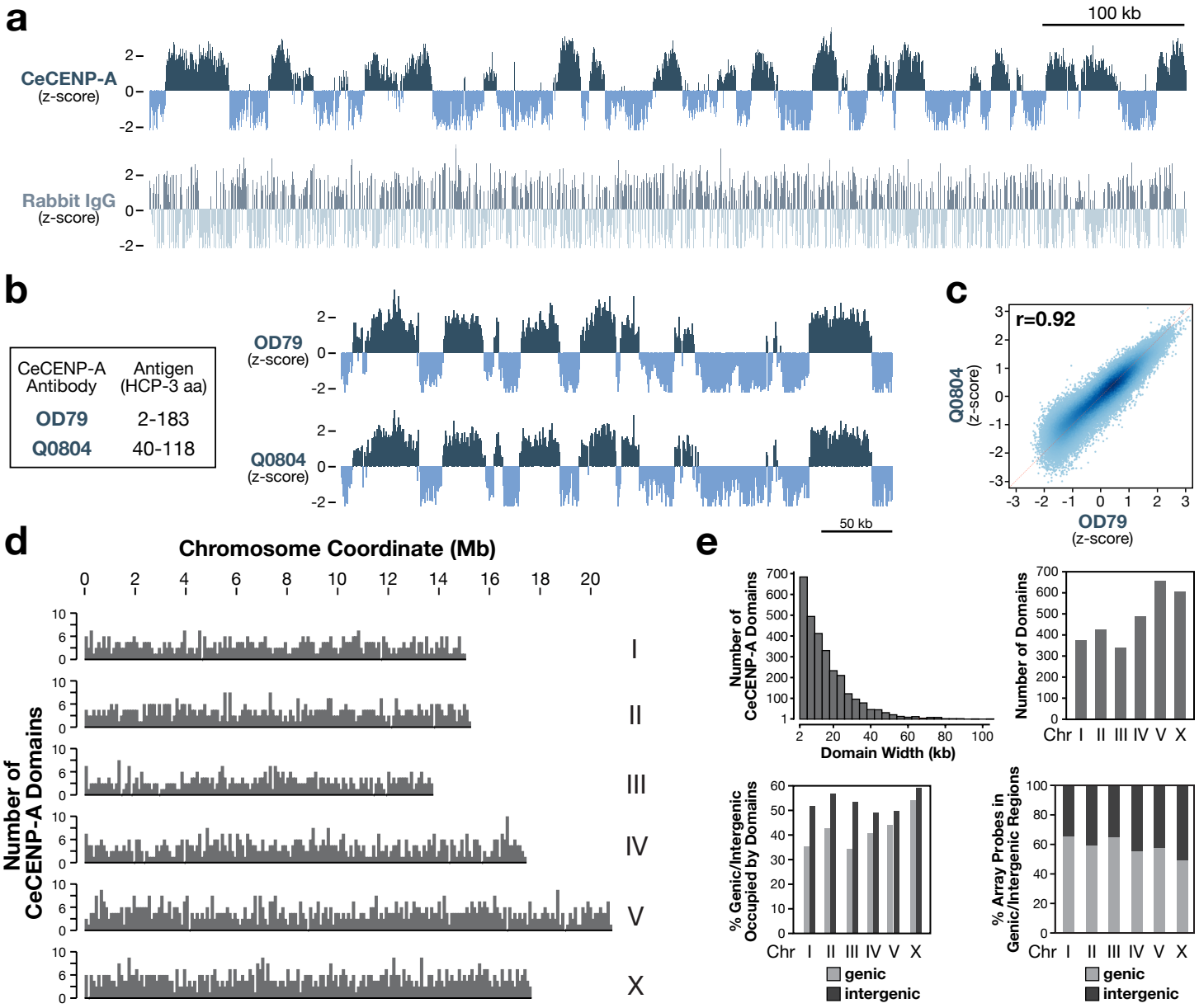

Figure S5: Analysis of CeCENP-A genome-wide ChIP-chip pattern.
(a) ChIP-chip pattern on a representative chromosomal region obtained with a specific anti-CeCENP-A antibody (OD79) and a random rabbit IgG control (1 replicate each).
(b) Average ChIP-chip patterns from two replicates on a representative chromosomal region obtained with two different antibodies generated against CeCENP-A (OD79 and SDQ0804). Antigens used for polyclonal antibody production in rabbits were located in the N-terminal tail and are indicated on the left. Antibody OD79 was used for all experiments described in the primary figures.
(c) Genome-wide correlation plot (probe level with 1-kb window average) of the two different CeCENP-A antibodies OD79 and SDQ0804. The signal for each antibody represents the average of two independent replicates.
(d) Distribution of CeCENP-A domains along each of the six chromosomes. The domain calling algorithm (see Methods) was used to define CeCENP-A domains on an average of two replicates genome-wide, and the number of domains within consecutive regions of 100kb were plotted for each chromosome.
(e) Additional CeCENP-A domain characteristics: number of domains as a function of domain size (*top left*), number of domains on individual chromosomes (*top right*) , genic/intergenic distribution of domains (*lower left*), and distribution of probes between genic and intergenic regions in the Nimblegen 2.1M probe tiling array (*lower right*). Genomic regions between transcript start sites and end sites in Wormbase (WS170) were annotated as genic and the rest of the genome as intergenic.
(f) CeCENP-A domain density does not correlate with repeat density. Repeats were downloaded from Wormbase. A vertical line on the right indicates 25 or more repeats in a 10-kb window. A vertical line on the left indicates at least 1 domain of CeCENP-A larger than 5kb in a 10-kb window. Repeats are strongly enriched on chromosome arms, whereas CeCENP-A domains are uniformly distributed along chromosomes.

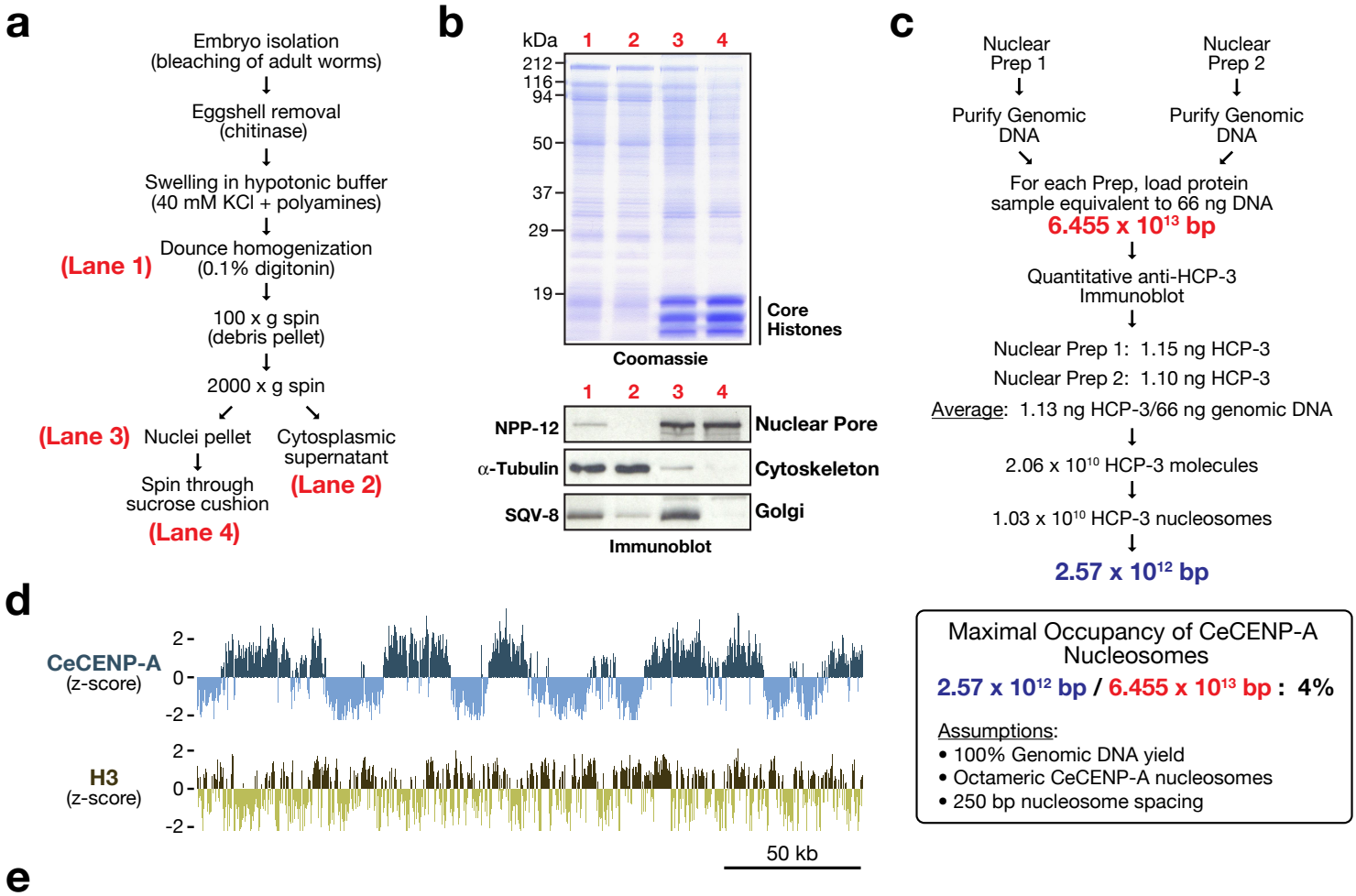

Figure S6: Quantifying the number of CeCENP-A molecules in nuclei to estimate fractional occupancy in CeCENP-A domains.

(a) Outline of the nuclei isolation procedure, starting from early embryos (< 100 cells) that were obtained by bleaching synchronized adult worms.

(b) Analysis of the cellular fractions obtained during preparation of nuclei. The abundant core histones are readily visible in the nuclear fractions by Coomassie staining. Immunoblotting confirms the presence of the nuclear pore complex protein NPP-12 in the nuclear fractions. By contrast, there is no significant amount of cytoplasmic α-tubulin. Spinning the isolated nuclei though a sucrose cushion reduces contamination with membranes, as illustrated by blotting for the Golgi marker SQV-8.

(c) Method used to determine the fractional occupancy of chromatin by CeCENP-A nucleosomes. Calculations were based on the amounts of CeCENP-A protein and genomic DNA in equivalent aliquots of nuclei, determined by quantitative immunoblotting and UV spectrometry, respectively. For the immunoblot, two independently generated nuclei preparations were used after loading was normalized to the DNA content in the two preparations. The result shows that there are only enough CeCENP-A molecules in nuclei to occupy ~4% of the genome with octameric CeCENP-A nucleosomes.

(d) ChIP-chip patterns of CeCENP-A and histone H3 showing that regions enriched for CeCENP-A also contain histone H3 signal. The histone H3 data were published previously[12].

(e) Genome-wide probe level correlation plot of CeCENP-A and histone H3 signals. There is no significant correlation between the two. The correlation coefficient (r) is indicated in the upper left.

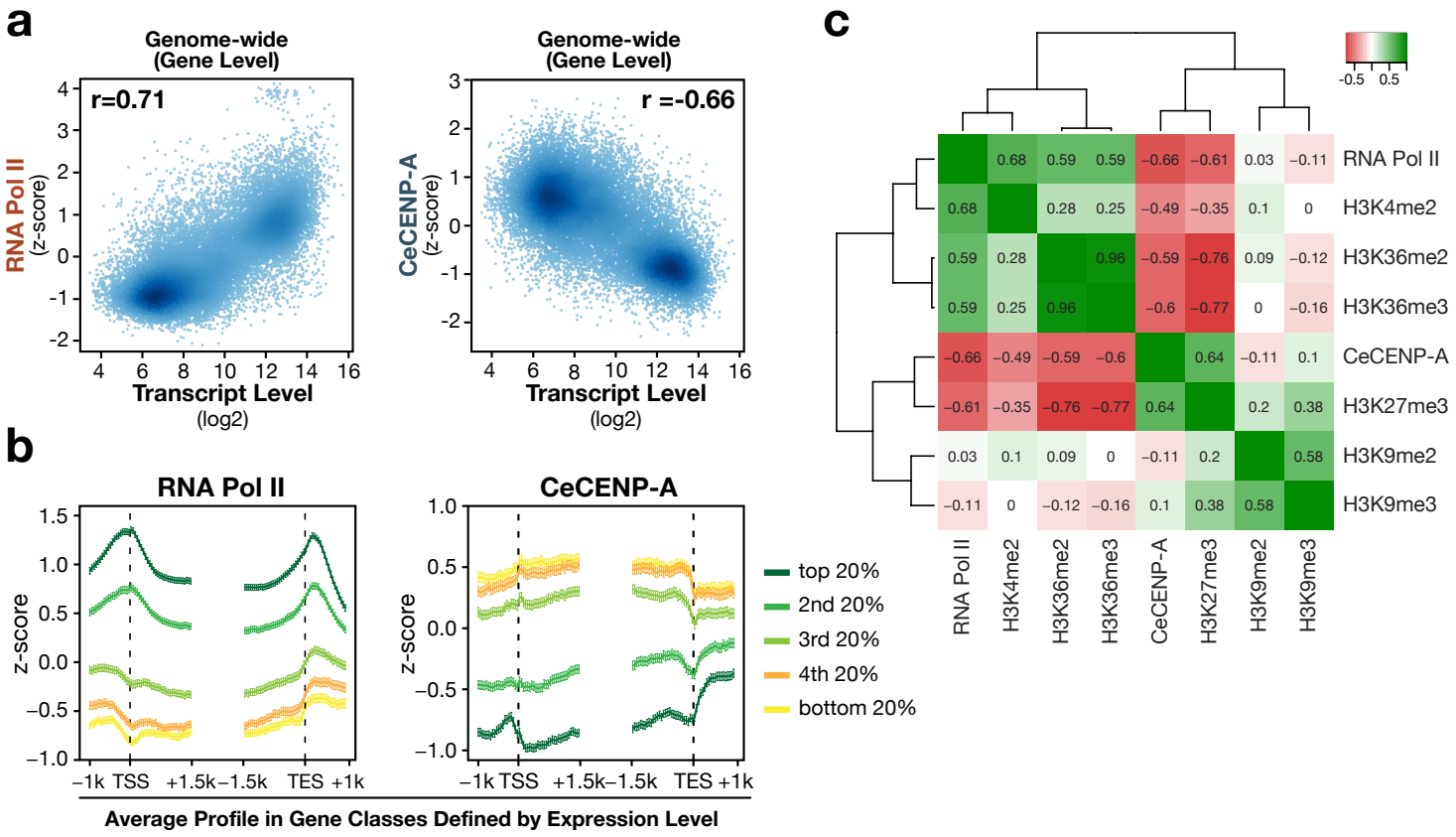

Figure S7: The inverse correlation between CeCENP-A and RNA Pol II occupancy is confirmed by analysis of transcript levels and histone tail modifications.

(a) Correlation plot of gene-level average z-scores for RNA Pol II or CeCENP-A versus transcript levels, illustrating the reciprocal relationship between CeCENP-A and gene expression. The correlation coefficients (r) are in the upper corners of the plots.

(b) Average profiles of RNA Pol II and CeCENP-A z-scores in gene classes defined by expression level. Genes > 2kb long (9932 genes) were grouped into five bins of equal size based on expression. Colors identify bins with highest (green) to lowest (yellow) transcript level in embryo extracts generated in parallel with ChIP extracts. Average z-score profiles for RNA Pol II and CeCENP-A ChIP-chip are shown in 50-bp steps in the 2.5kb around the transcript start site (TSS) and the transcript end site (TES). Error bars indicate 95% confidence intervals for the means.

(c) Heat map of Pearson correlation coefficients for ChIP-chip datasets of CeCENP-A, RNA Pol II, and histone modifications[9]. Correlations were calculated based on z-scores of all probes on the microarrays, after median smoothing over 1kb. Green indicates positive correlation, red indicates anti-correlation, and white indicates no correlation. Numbers within the cells indicate rounded correlation values.

The average of two independent replicates — where RNA Pol II ChIP-chip, CeCENP-A ChIP-chip and transcript analysis was performed for each replicate — was used for the analysis in *(a)* and *(b)*. The histone modification data used in *(c)* was generated from separate embryo extracts[9].

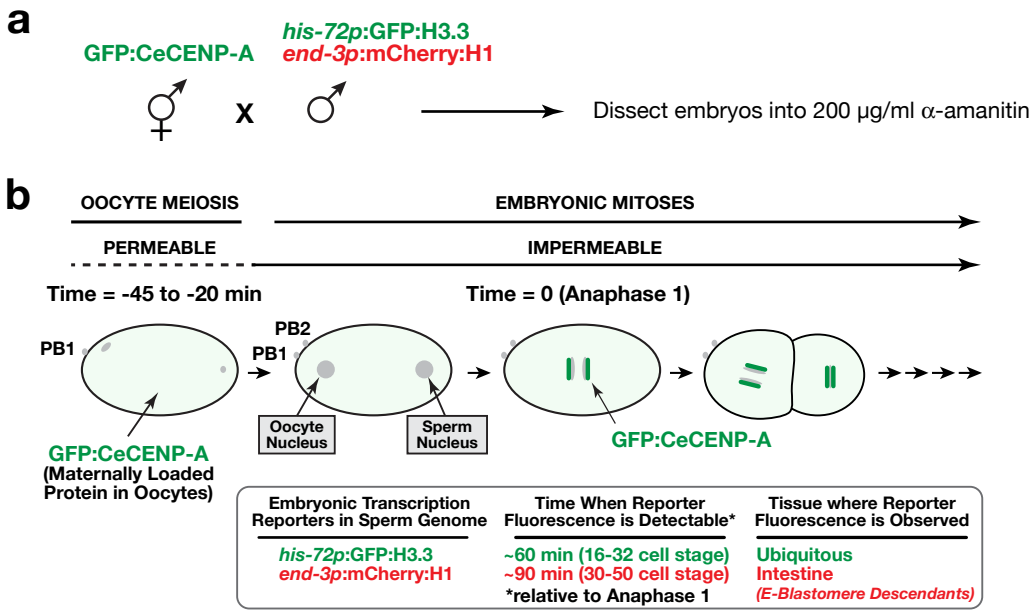

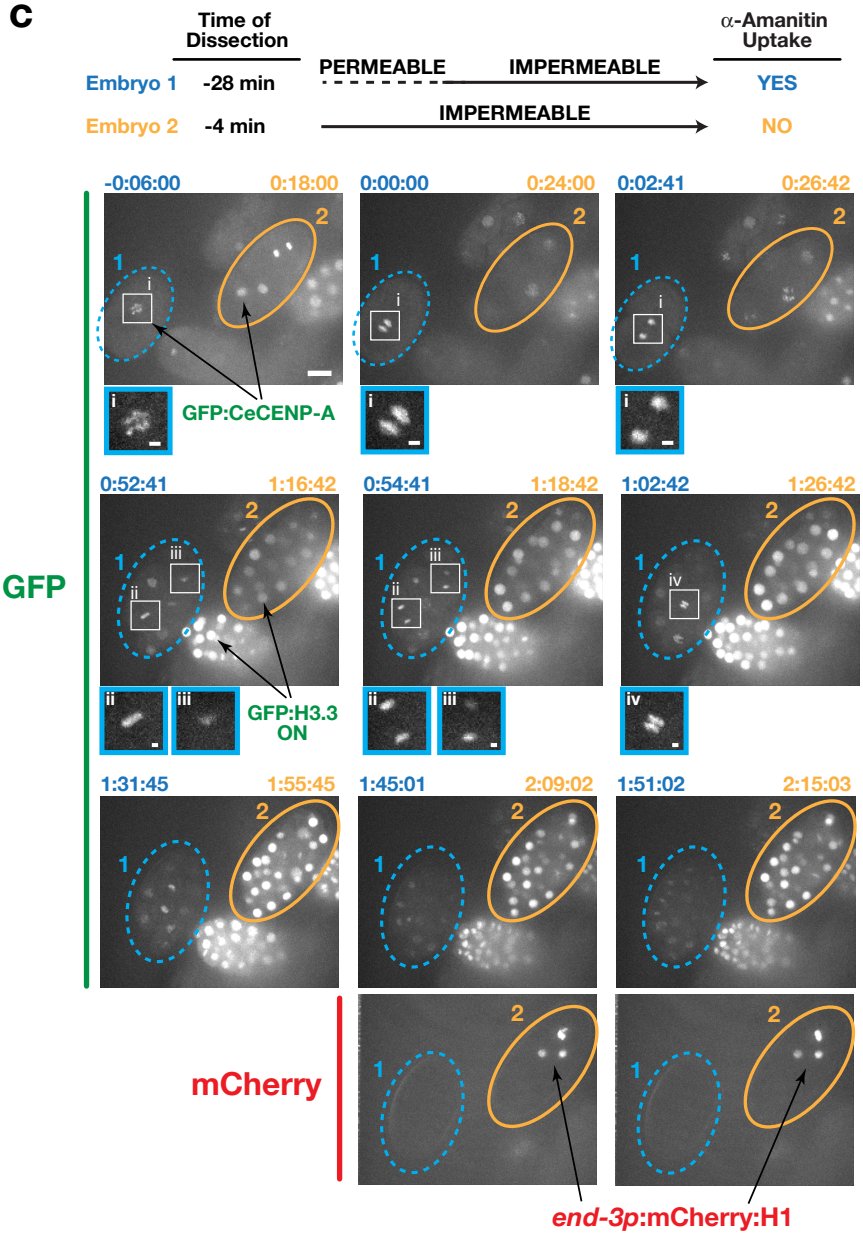

Figure S8: Chromosome segregation in early embryos is unaffected by inhibition of transcription.

(a) Mating scheme for experiment. Two transcription reporters are introduced via the sperm genome into oocytes expressing GFP:CeCENP-A before treatment of the fertilized embryos with α-amanitin.

(b) Schematic of the assay. Embryos can take up the transcriptional inhibitor α-amanitin until they complete oocyte meiotic divisions. Embryos exposed to α-amanitin after oocyte meiosis is completed are impermeable to the drug and serve as controls. In control embryos, the two transcription reporters present in the sperm genome turn on at ~60 and ~90 min after the first cleavage (Anaphase I). PB, polar body.

(c) Selected images from an experiment treating embryos with α-amanitin. Two embryos in the same field of view, one permeable at the time of dissection into medium containing α-amanitin (*Embryo 1*), the other already impermeable (*Embryo 2*), were filmed until they contained > 50 cells. In Embryo 2, the transcription reporter *his-72p:*GFP:histone H3.3 turns on as expected, whereas expression of this reporter is not observed in Embryo 1. Despite the lack of transcriptional activity in Embryo 1, chromosome segregation as monitored by GFP:CeCENP-A is unperturbed for multiple rounds of early embryonic divisions. Higher magnification views of GFP:CeCENP-A in Embryo 1 are shown below selected panels. The intestinal lineage transcription reporter *end-3p:*mCherry:histone H1 is activated in Embryo 2 but not in Embryo 1. Identical results were obtained for 4 permeable embryos, each of which was paired with an impermeable embryo in the same field of view as an internal control. Scale bar, 10 µm; higher magnification views, 2 µm.

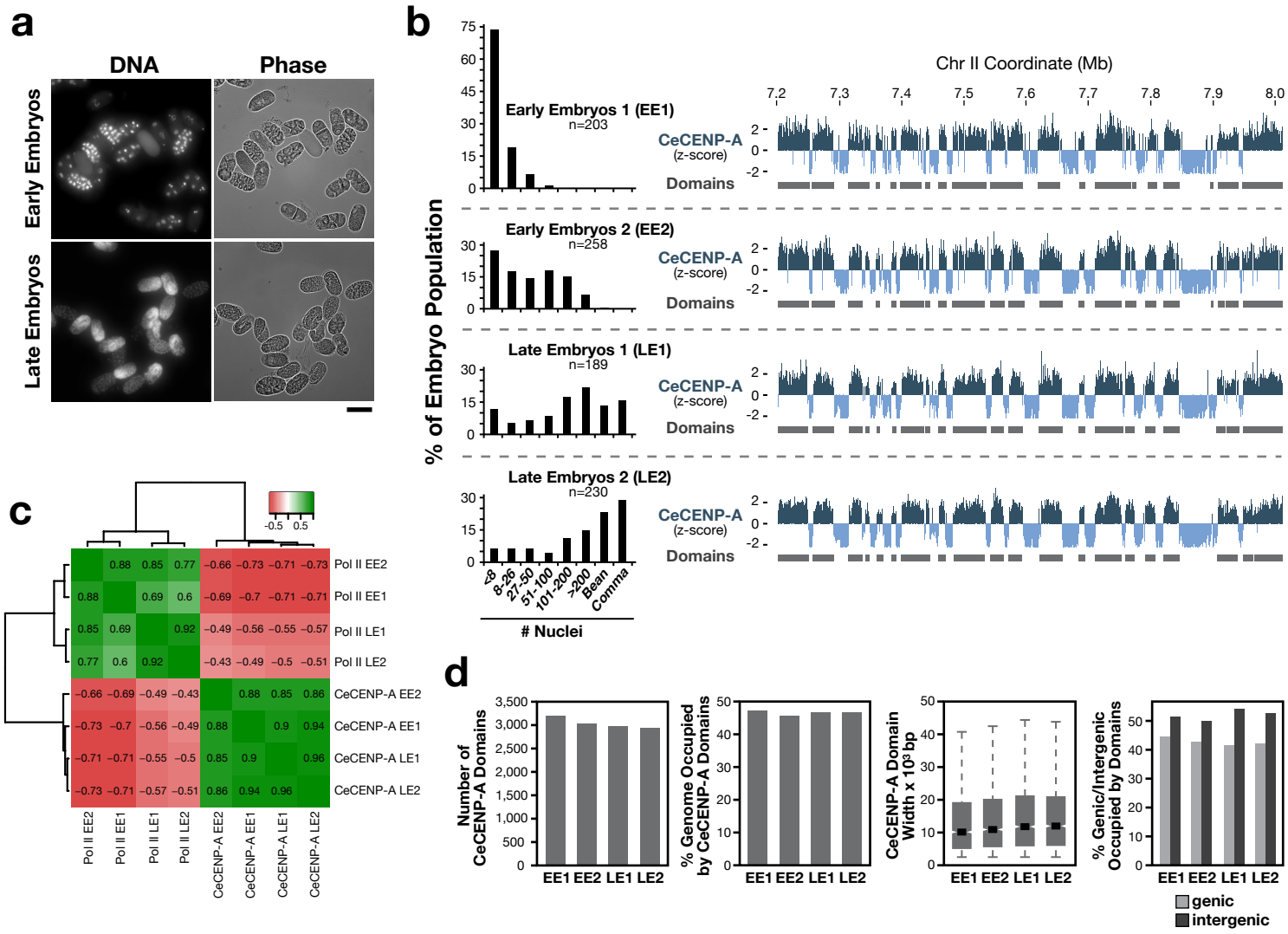

Figure S9: The distribution of CeCENP-A remains invariant during embryogenesis.
(a) Representative images of DAPI-stained embryos harvested from synchronized worms grown in liquid cultures, showing their developmentally distinct ages. Scale bar, 50 μm.
(b) Age distribution of embryos in the four developmentally staged ChIP extracts. Embryos were assigned to bins based on the number of DAPI-stained nuclei or embryo shape for late embryos. Representative genome browser views of the CeCENP-A ChIP-chip pattern in each extract and corresponding CeCENP-A domain calls are shown on the right.
(c) Heat map of Pearson correlation coefficients for CeCENP-A and RNA Pol II ChIP-chip datasets in the four developmentally staged extracts. Correlations were calculated based on z-scores of all probes on the microarrays, after median smoothing over 1kb. Green indicates positive correlation, red indicates anti-correlation, and white indicates no correlation. Numbers within the cells indicate rounded correlation values. Note the strong positive correlation between all four CeCENP-A datasets. In addition, negative correlation of the CeCENP-A datasets is strongest with the RNA Pol II early embryo datasets (correlation coefficients of -0.66 to -0.73) and is significantly weaker with RNA Pol II late embryo datasets (correlation coefficients of -0.43 to -0.51), which reflects the constancy of the CeCENP-A pattern despite changes in transcription during development.
(d) Number, size distribution, genome occupancy, and fraction of genic and intergenic regions occupied by CeCENP-A domains in each of the four developmentally staged embryo extracts. For the boxplots of domain width, each box extends from the 25th to 75th percentile, and the whiskers extending from a box indicate the 2.5th and 97.5th percentile. Wedges around the medians indicate a 95% confidence interval for the medians.

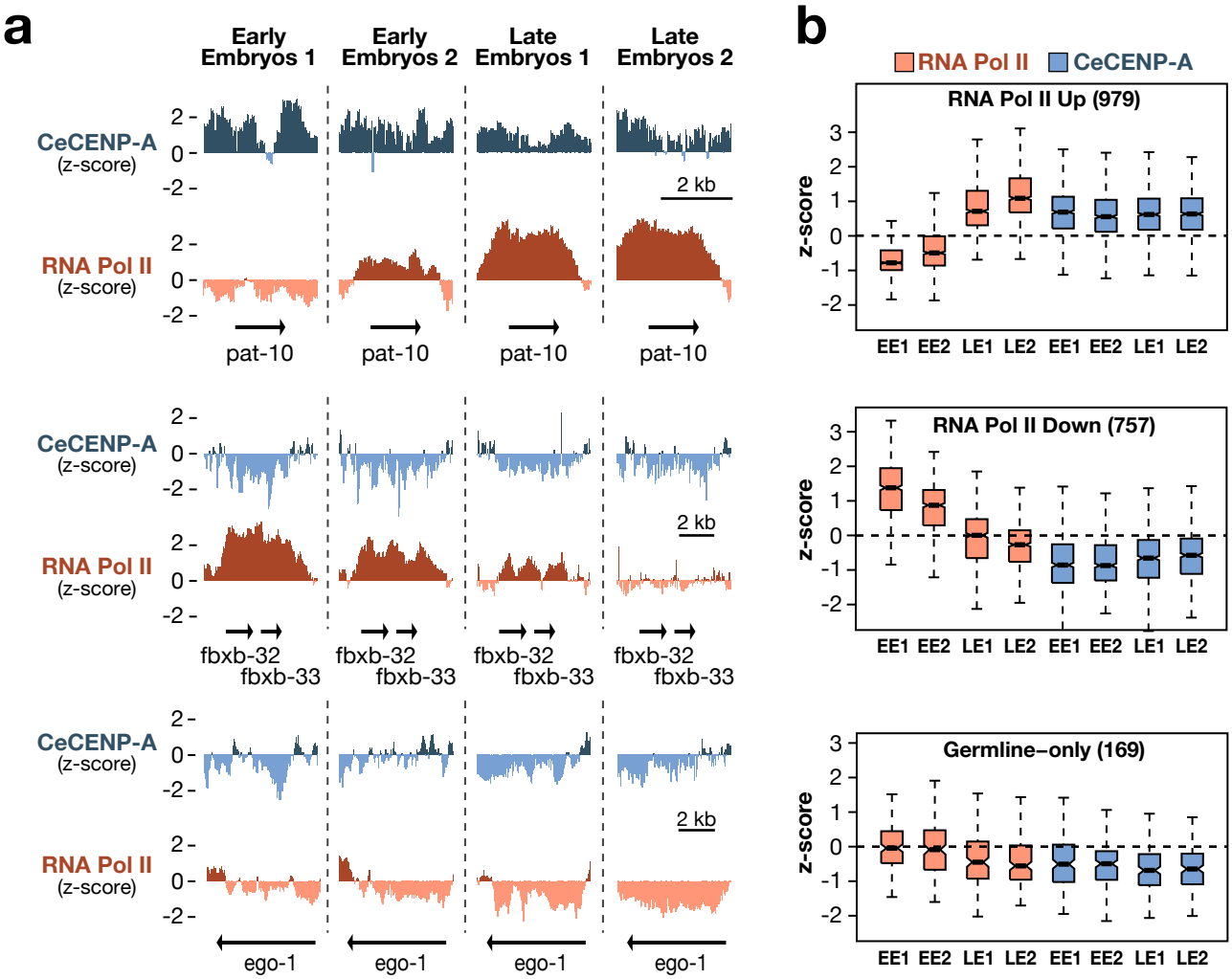

Figure S10: CeCENP-A does not change significantly on genes that alter expression during embryonic development and the embryo-expressed gene set exhibits low CeCENP-A occupancy.
(a) Examples of CeCENP-A and RNA Pol II distribution on genes for which RNA Pol II occupancy changes during embryogenesis, as well as for a "germline-only" gene.
(b) Boxplots (as in *Fig. S9d*) showing the range of RNA Pol II and CeCENP-A z-scores during the developmentally staged series for the "germline-only" gene set and for genes with significant changes in RNA Pol II levels between the early (average of EE1 and EE2) and late (average of LE1 and LE2) embryo extracts (see Methods). Note that for genes that show persistence of CeCENP-A signal despite acquisition of RNA Pol II signal in late embryos the interpretation is complicated by the fact that different cell types in the embryo may contribute RNA Pol II versus CeCENP-A signals. However, the lack of CeCENP-A acquisition on genes that turn off in late embryos and the lack of CeCENP-A acquisition on "germline-only" genes, which never acquire RNA Pol II signal throughout embryogenesis, both argue against CeCENP-A distribution simply reflecting active transcription. The number of genes in each set is shown in parentheses.
(c) Boxplot showing the range of RNA Pol II and CeCENP-A z-scores during the developmentally staged series for the "embryo-expressed" gene set, which is comprised of genes that are turned on early in embryogenesis (see Methods). Despite lack of the germline expression marker H3K36me3, the genes in this set have low CeCENP-A occupancy. This observation likely reflects removal of CeCENP-A by activation of transcription in early embryos.

a

WT vs. *met-1*:

132 domains > 5kb size with H3K36me3 increase > 1 z-score in *met-1* vs WT

↓

75 domains with RNA Pol II z-score < 0.1 in *met-1*

↓

Average ΔCENP-A$^{met-1 - WT}$ z-score = - 0.8

b

Examples of Ectopic H3K36me3 Domains:

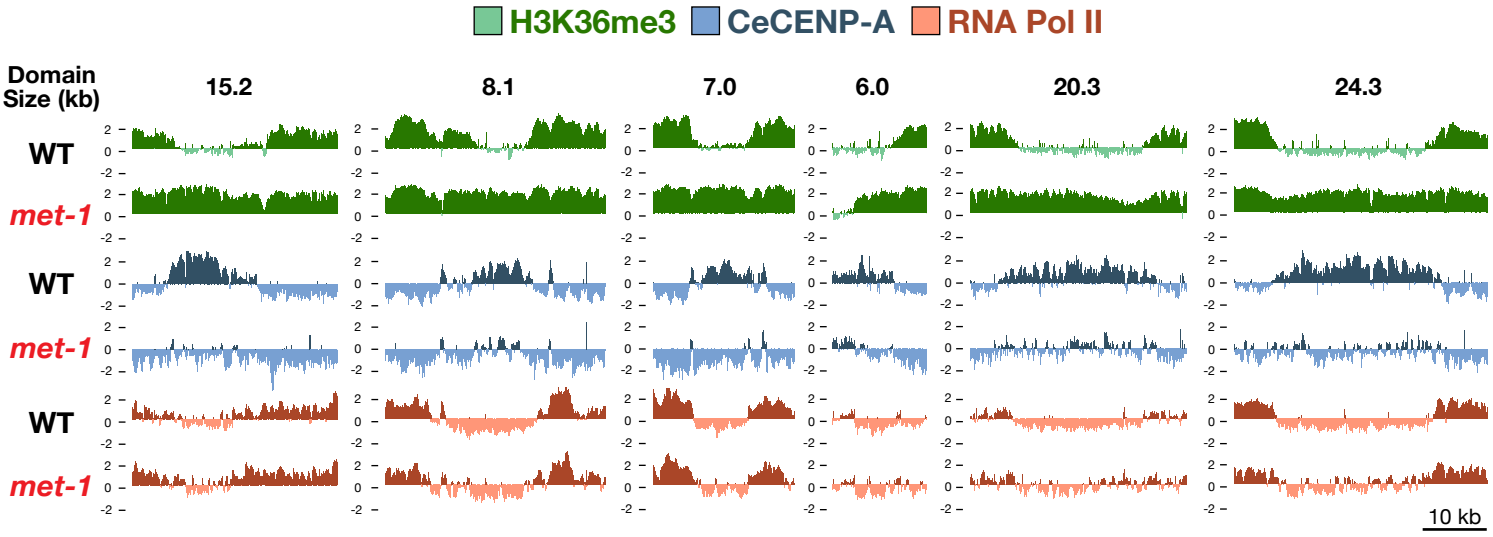

Figure S11: Ectopic H3K36me3 domains in *met-1* mutant embryos.
(a) Genome-wide analysis of H3K36me3 in *met-1* mutant and wild-type embryos using non-overlapping windows of 1kb revealed 132 regions >5kb in size in which the average H3K36me3 signal increased by more than 1 z-score in the *met-1* mutant. Despite significant loss of CeCENP-A (average signal decrease of -0.8 z-score), 75 of those regions did not have significant levels of RNA Pol II in either wild-type or *met-1* mutant embryos, suggesting that ectopic expression of these regions is likely restricted to the *met-1* mutant germline.
To identify these regions, the genome was segmented into 1 kb non-overlapping windows. Windows were identified as up for H3K36me3 in *met-1* mutant embryos if the difference in average z-score of H3K36me3 in *met-1* versus wild type was larger than 1. Neighboring windows with H3K36me3 up in *met-1* were combined into domains. 481 domains covering a total of 2.02 Mb were identified (using multiple biological replicates of wild type H3K36me3 as a control, we identified on average only 0.13 Mb of the genome having a pairwise difference in H3K36me3 of z > 1). 132 of these domains were larger than 5 kb and used to assess changes in CeCENP-A. Loss of H3K36me3 was also observed in the *met-1* mutant and will be described elsewhere, as this likely reflects MET-1 activity in embryos.
(b) Six examples of domains >5 kb with ectopic H3K36me3 signal in *met-1* embryos. CeCENP-A is lost from these regions in the absence of significant RNA Pol II signal in *met-1* embryos.

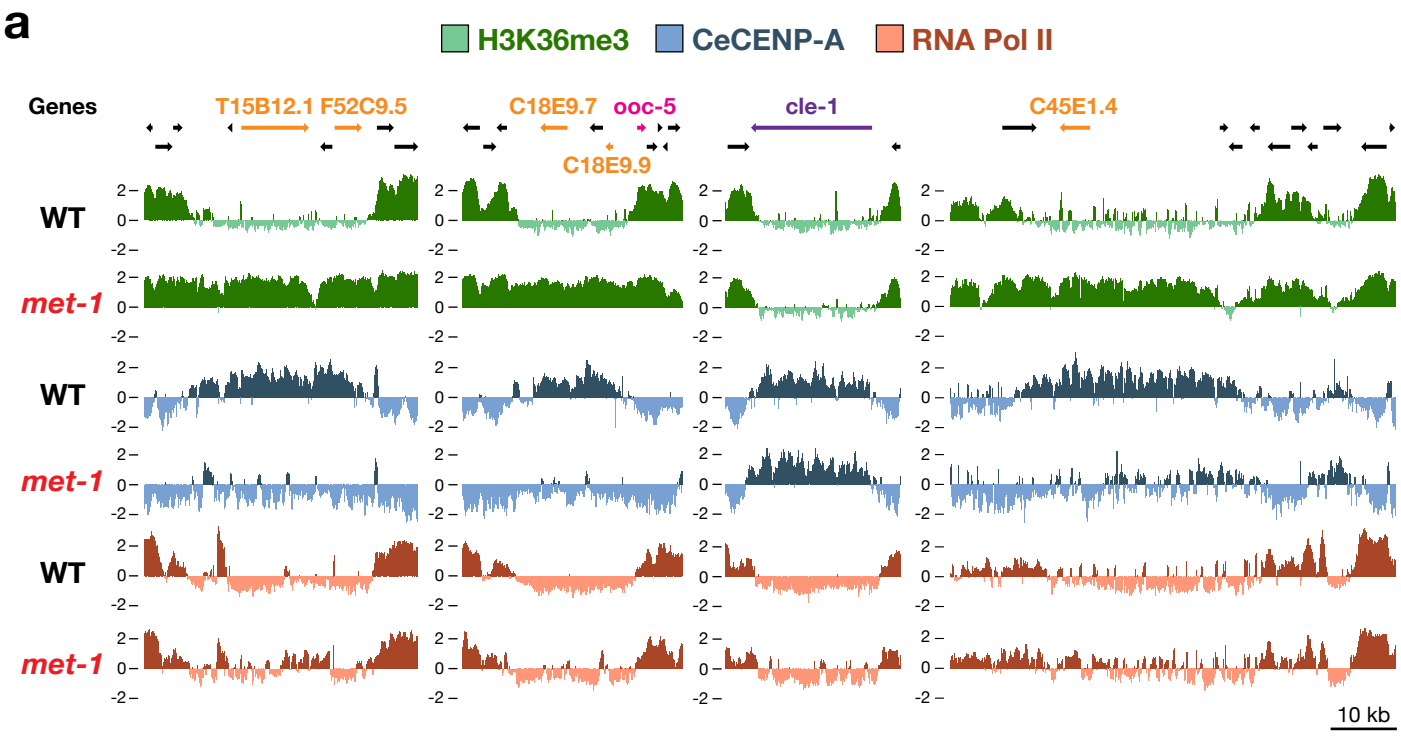

b

Expression Analysis in Dissected Germlines

Gene Name	H3K36me3 WT	H3K36me3 *met-1*	Expression Ratio *met-1* / WT (Mean ± SD)
ego-1	+	+	1 ± 0.2
ani-2	+	+	1 ± 0.2
gld-1	+	+	0.8 ± 0.3
ooc-5	+	+	1.1 ± 0.2
puf-5	+	+	0.9 ± 0.2
unc-15	-	-	1.3 ± 0.1
unc-13	-	-	2.1 ± 0.7
cle-1	-	-	1.3 ± 0.4
glb-18	-	+	35.2 ± 5.2
sol-1	-	+	369.9 ± 272.4
F26A3.5	-	+	22.3 ± 2.1
del-3	-	+	12.8 ± 1.4
C18E9.7	-	+	6.2 ± 2.8
C18E9.9	-	+	5.6 ± 2.6
C45E1.4	-	+	79.0 ± 27.2
T15B12.1	-	+	21.3 ± 5.4
F52C9.5	-	+	235 ± 58.9

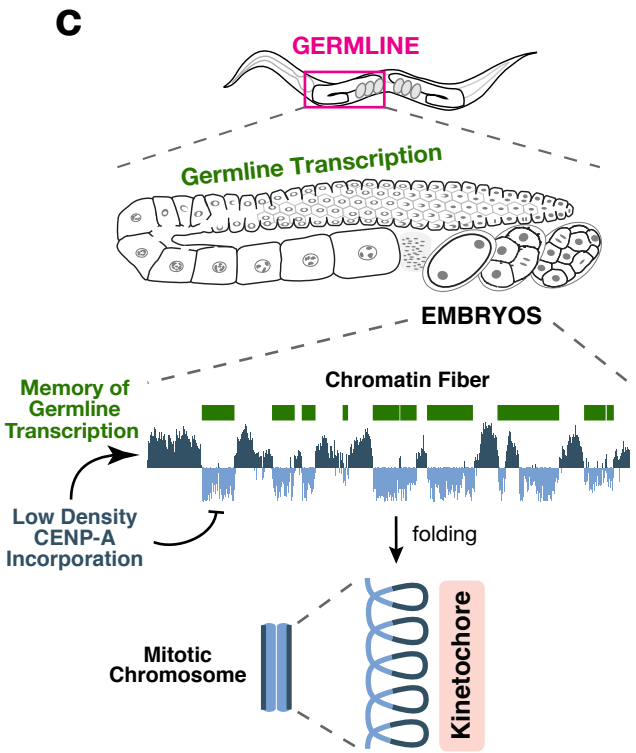

Figure S12: Ectopic germline transcription influences CeCENP-A occupancy in progeny embryos.
(a) Three regions with ectopic H3K36me3 signal in *met-1* mutant embryos with the location of genes indicated above the tracks.
(b) Expression analysis of genes in the regions shown in *(a)* and *Fig. 4b*. Real-time quantitative reverse transcription PCR was performed on hand-dissected wild-type and *met-1* mutant hermaphrodite gonads (4 independent biological replicates each).
(c) Speculative model: epigenetic memory of germline transcription restricts CeCENP-A deposition at fertilization in *C. elegans* embryos. CeCENP-A is excluded from regions transcribed in the maternal germline and loads at a low density in domains that were transcriptionally inactive in the germline. Coalescence of CeCENP-A domains into a stripe along each chromatid of a mitotic chromosome templates assembly of two sister kinetochores that are positioned opposite to one another. As embryo-expressed genes show low CeCENP-A occupancy (*Fig. S10c*), the initial germline transcription-guided pattern is likely remodeled and reinforced by activation of transcription in the early embryo.

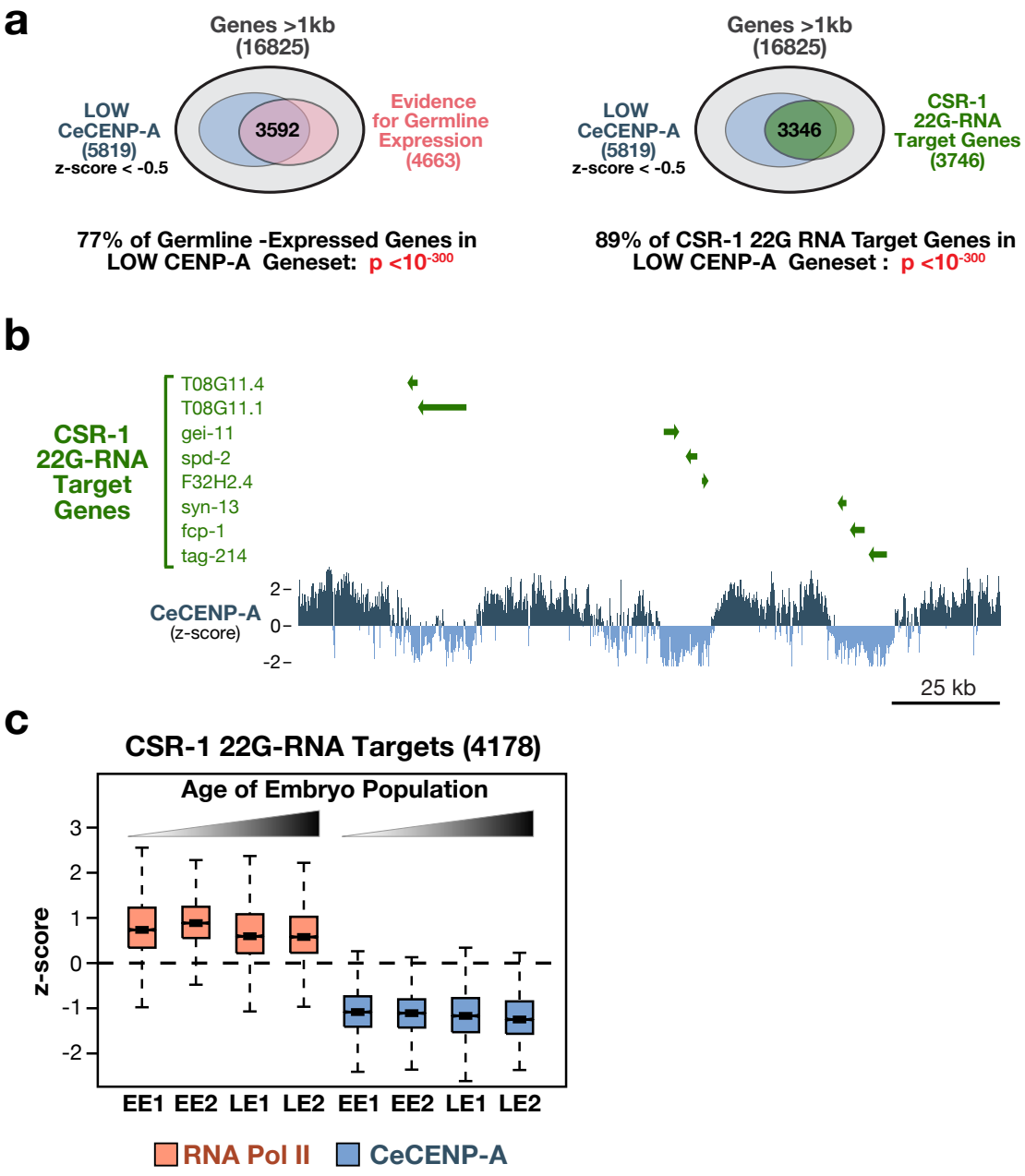

Figure S13: CeCENP-A is excluded from genes with homology to 22G-RNAs bound by the germline-specific Argonaut CSR-1.

(a) Venn diagrams showing significant overlap between genes with low CeCENP-A occupancy (z-score < -0.5), germline-expressed genes, and CSR-1 22G-RNA target genes. The Argonaut CSR-1 interacts with small RNAs (22G-RNAs) derived from genes transcribed in the germline and is proposed to bind to chromatin at 22G-RNA target loci[15]. Inhibition of CSR-1 or its co-factors results in chromosome segregation defects in early embryos[15,16].

(b) Genome browser view showing the reciprocal relationship between CeCENP-A permissive chromatin and CSR-1 22G-RNA target genes.

(c) Range of RNA Pol II and CeCENP-A z-scores shown as boxplots for genes with homology to 22G-RNAs bound to the Argonaute CSR-1 that were described previously[15].

Table S1: *C. elegans* strains used in this study.

Strain ID	Genotype
N2	Wild-type (ancestral N2 Bristol)
BA17	fem-1(hc17) IV
MT16973	met-1(n4337) I
RW10007	stIs10007[end-3(1kb):his-24:mCherry; unc-119(+)]; stIs10024; zuIs178 V [his-72(1kb 5' UTR):his-72:SRPVAT:GFP:his-72 (1KB 3' UTR) + 5.7 kb XbaI - HindIII unc-119(+)]
OD56	unc-119(ed3) III; ltIs37[pAA64; pie-1/mCherry:his-58; cb unc-119 (+)] IV
OD136	unc-119(ed3) III; ltIs115[pJM1; pie-1/GFP:hcp-3; cb unc-119 (+)]
OD265	unc-119(ed3) III; ltIs114[pJM12; pie-1/GFP:hcp-3; unc-119 (+)] I; hcp-3(ok1892) III/hT2[bli-4(e937) let-?(q782) qIs48] I,III; ltIs37[pAA64; pie-1/mCherry:his-58; unc-119 (+)] IV
OD347	unc-119(ed3); ltSi4[pOD833; hcp-3/GFP:hcp-3; cb unc-119(+)] II; hcp-3(ok1892) III
OD416	unc-119(ed3)III; ltSi98[pOD1097/pAM10; cpar-1/GFP:cpar-1; cb-unc-119(+)] II; ltIs37[pAA64; pie-1/mCherry:his-58; unc-119 (+)] IV
OD421	unc-119(ed3); ltSi4[pOD833; hcp-3/GFP:hcp-3; cb unc-119(+)] II; hcp-3(ok1892) III; ltIs37[pAA64; pie-1/mCherry:his-58; unc-119 (+)] IV
OD588	unc-119(ed3)III; ltSi98[pOD1097/pAM10; cpar-1/GFP:cpar-1; cb-unc-119(+)]II

Table S2: Primers for qPCR used in this study.

Gene	Name	Oligo 1	Oligo 2
T04C12.5	*act-2*	cgtcatcaaggagtcatggtc	catgtcgtcccagttggtaa
T15B12.1	T15B12.1	aggatgcacttttgcgttgga	cagaatgccatgccatcagc
F52C9.5	F52C9.5	atggctggggttcggaactt	cttcggcgcagtcttcgatt
C18E9.7	C18E9.7	atcgtaccgcgcatctccat	cggctcgcaggattccatta
C45E1.4	C45E1.4	acgtggactccgtgctgatg	gcggttgaactgtcggtgtg
C15A11.3	*sol-1*	acattgaaggttttaaccaa	atcattcgaaagtaattgga
F26A3.6	*del-3*	gaatacagaaccactcagga	cccaactgtaaaccatagag
F26A3.5	F26A3.5	aaagatggacaaaaacttca	gatccttccagtcatcaata
C18E9.9	C18E9.9	tattgaactcgcatacagtg	agaagttcttgaagcagaca
F52A8.4	*glb-18*	attagctcaagtggtcaaaa	atcgtctaaatcggtcataa
C18E9.11	*ooc-5*	tacaacgagaacatgtcaga	ggaagattcagggaagtatt
F54C9.8	*puf-5*	tgtcttctccgtaacattct	gtctcctgatccttcacata
K10B2.5	*ani-2*	aacatatgcatttctcgaat	acaggacactgttgtttctc
F26A3.3	*ego-1*	aaagaagatgaaatcgatga	atccatattggtcagaattg
T23G11.3	*gld-1*	tacgtagttcaggtccagtt	gagagctgaatgaatcaaac
ZK524.2	*unc-13*	atatggcaagagaatctgaa	gcatatttgagagattggag
F07A5.7	*unc-15*	ggttcttatcgttgatcttg	tgtctctcgagttgttctct
C36B1.1	*cle-1*	aagcatctttaaatgcagac	ttatccattggcttgatagt

Table S3: Microarray data used in this study.

ChIP-chip

Target	Source	Source ID	Strain	Embryo Stage[a]	Accession Number[b]	Shown in Figures	Reference
CeCENP-A	Desai	OD79	N2	Early (EE1&EE2)	modENCODE_3540	3a-c; S6; S7; S9; S10; S13	this study
CeCENP-A	Desai	OD79	N2	Late (LE1&LE2)	modENCODE_3542	2; 3d-f; S5; S9; S10	this study
CeCENP-A	Desai	OD79	N2	Early	modENCODE_2541	4; S11; S12	this study
CeCENP-A	Desai	OD79	MT16973	Early	GSE35079	4; S11; S12	this study
CeCENP-A	SDI	SDQ0804	N2	Late (LE1&LE2)	modENCODE_3543	S5b, c	this study
KNL-2	SDI	SDQ0803	N2	Late (LE1)	modENCODE_4619	2a, b	this study
KNL-2	SDI	SDQ0810	N2	Late	modENCODE_4620	2a, b	this study
RNA Pol II	Abcam	ab817	N2	Early (EE1&EE2)	modENCODE_3544	3a-c; S7; S9; S10; S13	this study
RNA Pol II	Abcam	ab817	N2	Late (LE1&LE2)	modENCODE_3545	3d-f; S9; S10	this study
RNA Pol II	Abcam	ab817	N2	Early	modENCODE_663	4; S11; S12	(9)
RNA Pol II	Abcam	ab817	MT16973	Early	GSE35079	4; S11; S12	this study
H3K36me3	Kimura	13C9	N2	Early	modENCODE_973	4; S11; S12	(9)
H3K36me3	Kimura	13C9	MT16973	Early	GSE35079	4; S11; S12	this study
H3	Active Motif	AR-0144	N2	Early	modENCODE_2312	S6	(13)

Expression Profiling

Sample	Strain	Embryo Stage	Accession Number	Shown in Figure	Reference
Total RNA	N2	Early (EE1&EE2)	modENCODE_4621	S7	this study

[a] EE1, EE2, LE1, and LE2 refer to specific embryo extracts.

[b] www.modencode.org/; www.ncbi.nlm.nih.gov/geo/

Supplemental Discussion

The inverse correlation between CeCENP-A and RNA Pol II occupancy/transcript levels in embryos (**Fig. 3a-d**; **Fig. S7**) immediately suggested that active transcription accounts for the CeCENP-A genome-wide pattern. In this model, CeCENP-A is uniformly incorporated throughout the genome but continually removed from genomic regions that are being transcribed. However, several observations are inconsistent with this model. The one-cell embryo does not have detectable RNA Pol II-dependent transcription[10-12] and, as shown here, the sperm nucleus enters the embryo without detectable CeCENP-A (**Fig. 1b, c; Fig. S2b**). Nevertheless, at the resolution of cytology, the distribution of CeCENP-A on the chromosomes that originated in the sperm is not uniform during the first division but instead resembles the restricted pattern seen on the chromosomes from the oocyte (**Fig. 1d** and ref *(21)*; the sperm and oocyte chromosomes do not mix until after anaphase in the one-cell *C. elegans* embryo, so one half of the metaphase plate is sperm chromatin and the other half is oocyte chromatin). This observation suggested that CeCENP-A incorporation could be restricted to specific genomic regions in the absence of genome-wide transcription and without prior presence of CeCENP-A nucleosomes. In addition, mapping CeCENP-A genome-wide during progressively later stages of embryonic development revealed a remarkable constancy of the CeCENP-A pattern, despite significant changes in RNA Pol II occupancy (**Fig. S10a**, **b**). Finally, inhibiting transcription with α-amanitin did not affect the cytological pattern of CeCENP-A or impair chromosome segregation in the early embryo (**Fig. S8**). Because α-amanitin has to be added to embryos during the first

meiotic division before the impermeable eggshell has formed, we were unable to perform this experiment on a large scale to map CeCENP-A localization by ChIP. Thus, it remains possible that the genome-wide distribution of CeCENP-A was affected under this experimental condition.

The above findings led us to explore potential alternative cues directing targeting of CeCENP-A to specific genomic regions. We observed that germline-expressed genes are highly enriched in genomic regions lacking CeCENP-A (**Fig. S13a**), and a set of 169 genes that are transcribed exclusively in the germline but not in embryos ("germline-only") failed to load CeCENP-A throughout embryogenesis despite their transcriptional inactivity (**Fig. S10a, b**). The latter observation was bolstered by individual inspection of well-studied genes known to be transcribed only in the germline (e.g. genes involved in processes such as meiosis, RNP granule biogenesis, eggshell synthesis, etc.) that were not present in the germline-only gene set, which was defined using publicly available expression data. These observations suggested that transcription in the germline defines regions as non-permissive for CeCENP-A incorporation in the progeny. A chance observation in the *met-1* null mutant provided support for this idea: ectopic transcription of some genes in the germline of this viable mutant correlated with a decrease of CeCENP-A occupancy in embryos. Of note, the effect on CeCENP-A was observed in the absence of significant RNA Pol II occupancy in embryos (**Figs. 4, S11, S12**), arguing against the observed change being due to embryonic transcription. Thus, the strong enrichment of germline-expressed genes in genomic regions depleted of CeCENP-A in embryos, the inability of "germline-only"

genes to incorporate CeCENP-A throughout embryogenesis, and the effect of ectopic germline transcription on CeCENP-A occupancy in embryos all suggest that germline transcription is involved in patterning the genome for CeCENP-A occupancy in the progeny. We speculate that epigenetic memory of germline transcription restricts CeCENP-A incorporation in the genome immediately after fertilization and that this represents the initial basal CeCENP-A pattern that directs chromosome segregation (**Fig. S12c**).

While the data summarized above links germline transcription to patterning CeCENP-A deposition in the embryo, germline transcription is insufficient to explain the full genome-wide CeCENP-A pattern, as genes expressed early in embryogenesis were depleted of CeCENP-A even though they lacked signatures of germline expression (**Fig. S10c**). Thus, we propose that the initial definition at fertilization of genomic regions permissive for CENP-A incorporation is based on germline transcription and that activation of transcription during early embryogenesis remodels and reinforces this basal pattern.